

Hexamolybdenum Clusters Supported on Exfoliated h-BN Nanosheets for Photocatalytic Water Purification

Mariia N. Ivanova,* Yuri A. Vorotnikov, Elena E. Plotnikova, Margarita V. Marchuk, Anton A. Ivanov, Igor P. Asanov, Alphiya R. Tsygankova, Ekaterina D. Grayfer,* Vladimir E. Fedorov, and Michael A. Shestopalov



Cite This: <https://dx.doi.org/10.1021/acs.inorgchem.0c00528>



Read Online

ACCESS |



Metrics & More

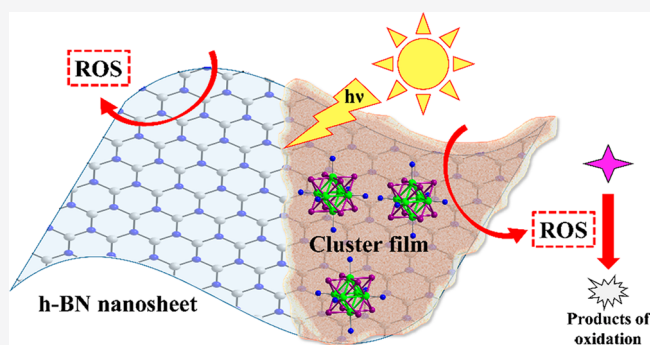


Article Recommendations



Supporting Information

ABSTRACT: Nowadays, the development of new effective photocatalytic materials for the purification of real wastewaters and model systems containing organic molecules constitutes an important challenge. Here we present a preparation strategy for composite materials based on hexamolybdenum cluster complexes and exfoliated hexagonal boron nitride (h-BN) nanosheets. Cluster deposition on the nanosheet surface was achieved by impregnation of the matrix by a $(\text{Bu}_4\text{N})_2[\{\text{Mo}_6\text{I}_8\}(\text{NO}_3)_6]$ /acetone solution. Successful cluster immobilization and chemical composition of the samples were verified by inductively coupled plasma atomic emission spectroscopy, transmission electron microscopy with elemental mapping (TEM/EDS), X-ray photoelectron spectroscopy (XPS), and optical diffuse-reflectance spectroscopy. A small amount of water in acetone initiates the hydrolysis of a molybdenum cluster precursor with labile NO_3^- ligands, which are absent in the final composite, according to the XPS data. Intermediate hydrolyzed cluster forms anchor to the surface of h-BN nanosheets and promote growth of the insoluble compound $[\{\text{Mo}_6\text{I}_8\}(\text{H}_2\text{O})_2(\text{OH})_4]\cdot\gamma\text{H}_2\text{O}$ as the final hydrolysis product. TEM/EDS proves that the cluster exists at the nanosheet surface in the form of an X-ray diffraction amorphous thin film. The samples obtained show high photocatalytic activity in the degradation of a model pollutant rhodamine B under UV- and visible-light irradiation. The materials retain their initial photocatalytic efficacy during at least six cycles without the need for recovery.



INTRODUCTION

In the last few decades, a global problem of water pollution by industrial products requires new effective ways of wastewater purification. Especially, a photocatalytic approach seems to be the most powerful and sustainable tool for the degradation of organic pollutants, owing to its numerous advantages, including the use of sunlight as a renewable energy source, photocatalyst recycling without activity loss, etc. Therefore, huge efforts have been made to develop new effective photocatalytic materials with the required characteristics, such as high activity, chemical stability, cost efficiency, easy recyclability, and a range of working wavelengths close to sunlight.^{1,2} Usually, TiO_2 -based materials were studied in this context,³ but they have a major disadvantage of acting effectively only under UV-light irradiation, i.e., utilizing less than 10% of the sunlight spectrum. Many other materials have been developed, but the task is still challenging.^{1–6}

On the basis of our broad experience with octahedral transition-metal cluster complexes, particularly, molybdenum clusters $[\{\text{Mo}_6\text{X}_8\}\text{L}_6]^n$ ($\text{X} = \text{Cl}, \text{Br}, \text{or I}$; $\text{L} = \text{organic or inorganic ligands}$; Figure 1),^{7–18} we suggest considering them as promising agents for photocatalytic water purification. Their

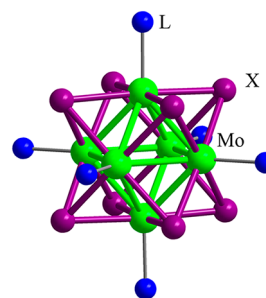


Figure 1. Representation of the hexamolybdenum clusters $[\{\text{Mo}_6\text{X}_8\}\text{L}_6]^n$. Color code: Mo, green; X, purple; L, blue.

Received: February 19, 2020

variable terminal ligand (L) environment provides for chemical reactivity and solubility, while the highly stable cluster core $\{\text{Mo}_6\text{X}_8\}^{4+}$ is responsible for the photophysical properties, i.e., photoluminescence^{16–19} and the ability to generate reactive oxygen species (ROS), such as singlet oxygen, hydroxyl radical, superoxide radical, etc.^{13,14,20–23} Owing to these beneficial characteristics, this class of compounds is already well-studied for numerous applications, including as components of optical waveguides,¹² liquid-crystal devices,²⁴ solar panels,²⁵ antibacterial materials,^{26,27} agents for bioimaging^{22,28} and photodynamic therapy,^{9,10,13,14,22} and catalysts.^{29–31} However, the water treatment processes employing hexamolybdenum cluster complexes remain little explored. To the best of our knowledge, the only two examples are the studies on rhodamine B (RhB) photodegradation in water using a $[\{\text{Mo}_6\text{Br}_8\}(\text{N}_3)_6]^{2-}$ cluster as a homogeneous catalyst²¹ or a heterogeneous one when combined with gold nanoparticles and graphene oxide as the support.²⁰ However, a simple two-component system containing a cluster and a support for heterogeneous photocatalysis has not been described. At the same time, cluster complexes have been often combined with various matrixes beyond graphene oxide,^{20,29,30} such as MIL-101⁹ and SiO_2 meso- and nanoparticles,^{13–15,28,32–34} polystyrene,^{8,10,16,26,27,35} polyurethane,³⁶ poly(methyl methacrylate),^{12,37–39} and poly(vinylpyrrolidone).⁴⁰

In our work, we propose another matrix, hexagonal boron nitride (h-BN), to anchor cluster complexes and promote their application in photocatalytic water purification processes. h-BN is a layered material with a crystal structure quite similar to that of graphite but an isolator in its physical nature, so it is called “white graphite”. h-BN is known to have high thermal conductivity, stability toward high temperatures and aggressive chemical conditions (acids, bases, and oxidants), transparency in the visible and near-UV range, etc. Furthermore, recently it was shown that h-BN itself possesses catalytic activity in certain processes^{2,41–45} and participates in photocatalysis by separating charge carriers, e.g., holes and electrons.^{2,46} Therefore, h-BN nanosheets were used as supports for photocatalytically active particles, such as anatase (TiO_2),⁴⁷ TiO_2/Au ,^{48,49} graphitic carbon nitride ($\text{g-C}_3\text{N}_4$),^{2,46} etc.

Thus, this work is aimed at the preparation and characterization of composite materials based on 2D h-BN nanosheets (BNNS) with octahedral molybdenum cluster complexes and investigation of their photocatalytic properties in the reactions of organic dye degradation under UV- or visible-light irradiation. Moreover, the composition, morphology, and photocatalytic properties of the obtained materials were comprehensively investigated.

EXPERIMENTAL SECTION

Materials and Methods. h-BN powder (1 μm in size and $\geq 98.0\%$ purity) and RhB were purchased from Sigma-Aldrich. Molybdenum powder was annealed in a hydrogen flow and had $\geq 99.9\%$ purity. $(\text{Bu}_4\text{N})_2[\{\text{Mo}_6\text{I}_8\}\text{I}_6]$ and $(\text{Bu}_4\text{N})_2[\{\text{Mo}_6\text{I}_8\}(\text{NO}_3)_6]$ were obtained according to previously reported procedures.^{16,50} Other reagents and solvents were commercially available and were used without additional purification. Acetone contained some moisture.

Ultrasonic treatment was carried out in a “Sapphire” ultrasonic bath (ultrasound power 150 W; frequency 35 kHz). Centrifugation was achieved by a Beckman Coulter Allegra X-30 centrifuge equipped with rotor F0630 (acceleration of 20000g). UV-light irradiation was performed by a Hamamatsu Photonics light-emitting-diode (LED) head unit L11921-400 (wavelength 365 ± 5 nm) used with a LED

controller C11924-211 (670 mW). Visible-light irradiation was carried out by an IKEA LED lamp (110 mW; wavelength range ~ 400 – 700 nm; Figure S1).

Powder X-ray diffraction (XRD) patterns for solid samples were collected using a Philips PW 1830/1710 automated diffractometer (Cu $K\alpha$ radiation, graphite monochromator, and silicon plate as an external standard). High-resolution transmission electron microscopy (HRTEM) images were obtained with a JEOL JEM-2200FS microscope with a lattice-fringe resolution of 0.1 nm at an accelerating voltage of 200 kV. Suspensions in ethanol were deposited on carbon-film-coated copper grids. UV-vis absorption spectra were collected by an Agilent Cary 60 automatic spectrophotometer.

To determine the molybdenum content in nanocomposite samples, inductively coupled plasma atomic emission spectroscopy (ICP-AES) analyses of solutions prepared by microwave-assisted washing of molybdenum from a BN matrix ($\text{HF}:\text{H}_2\text{O}_2 = 1:0.15$; 150 – 180 °C) were carried out on a Thermo Scientific iCAP-6500 high-resolution spectrometer with a cyclone-type spray chamber and a “SeaSpray” nebulizer. The spectra were obtained by axial plasma viewing. Standard operating conditions of the ICP-AES system were as follows: power = 1150 W, injector inner diameter = 3 mm, carrier argon flow = 0.7 L min^{-1} , accessory argon flow = 0.5 L min^{-1} , cooling argon flow = 12 L min^{-1} , number of parallel measurements = 3, and integration time = 5 s. Deionized water ($R \approx 18$ M Ω) was used to prepare the sample solutions.

Optical diffuse-reflectance spectra were measured at room temperature on a Shimadzu UV-vis-near-IR 3101 PC spectrophotometer equipped with an integrating sphere and reproduced in the form of Kubelka–Munk theory. To determine the band gap (E_g) of the samples, the Tauc plot method $[(h\nu\alpha)^{1/2} = A(h\nu - E_g)]$, where h = Planck constant, ν = frequency, α = absorption coefficient, and A = proportionality constant] was used.

X-ray photoelectron spectroscopy (XPS) was performed on a SPECS Phoibos-150 multi channeltron detector (MCD) spectrometer with monochromatic Al $K\alpha$ excitation. The electron pass energy was 20 eV. The powder samples were pressed into double-sided adhesive carbon tape. For neutralization of the charging effect, irradiation of the samples by a low-energy electron beam was applied. Calibration of the binding energies was performed relative to an internal standard from the C 1s to 285.0 eV. Separation of the contributions from different atoms was carried out by a fitting of spectra on mixed Lorentzian–Gaussian symmetrical components.

Synthetic Procedures. Preparation of Exfoliated BNNS. h-BN nanosheets were prepared by the treatment of h-BN powders with H_2O_2 (30%) following a modified technique.⁵¹ Typically, 150 mg of h-BN was put into a cylindrical Teflon autoclave (rated pressure 2–3 atm). A total of 30 mL of a H_2O_2 solution was added, and the mixture was ultrasonicated for 30 min and then thermostated in a water bath for 20 h at 80 °C. After the reaction, the solid phase of the mixture was separated by centrifugation, washed two times with distilled water and ethanol, and then dried at 50 °C until a constant mass was reached.

Impregnation of BNNS with $(\text{Bu}_4\text{N})_2[\{\text{Mo}_6\text{I}_8\}\text{I}_6]$. $(\text{Bu}_4\text{N})_2[\{\text{Mo}_6\text{I}_8\}\text{I}_6]$ (228 mg, 80 μmol) and BNNS (100 mg, 4.0 mmol) with a molar ratio of 0.02:1 were placed in a flask, 100 mL of acetone was added, and the mixture was ultrasonicated for 1 h. Then the precipitate was isolated by centrifugation, washed with acetone three times, and dried in air at 50 °C until a constant mass was reached.

Preparation of AH_x/BNNS Composites by In Situ Hydrolysis of $(\text{Bu}_4\text{N})_2[\{\text{Mo}_6\text{I}_8\}(\text{NO}_3)_6]$ in the Presence of BNNS. A total of 100 mg of BNNS and 100 mL of acetone were mixed in a flask, and different amounts of $(\text{Bu}_4\text{N})_2[\{\text{Mo}_6\text{I}_8\}(\text{NO}_3)_6]$ were added: 10, 50, 100, 200, 300, and 500 mg [the molar ratios of $(\text{Bu}_4\text{N})_2[\{\text{Mo}_6\text{I}_8\}(\text{NO}_3)_6]/\text{BNNS}$ were 0.001:1, 0.005:1, 0.01:1, 0.02:1, 0.03:1, and 0.05:1, respectively], which was followed by ultrasonication for 5 h. Then the precipitate was isolated by centrifugation, washed with acetone three times, and dried in air at 50 °C until a constant mass was reached. The samples are referred to as AH_x/BNNS (x is the moles of $(\text{Bu}_4\text{N})_2[\{\text{Mo}_6\text{I}_8\}(\text{NO}_3)_6]$ on 1 mol of BNNS).

Preparation of Bulk $[(\text{Mo}_6\text{I}_8)(\text{H}_2\text{O})_2(\text{OH})_4]\cdot y\text{H}_2\text{O}$ (bAH). A total of 300 mg of $(\text{Bu}_4\text{N})_2[(\text{Mo}_6\text{I}_8)(\text{NO}_3)_6]$ was dissolved in acetone (19 mL) containing some moisture, and $\text{NH}_3\cdot\text{H}_2\text{O}$ (1.9 mL) was added under constant stirring. The mixture was stirred for 24 h to achieve full precipitation. The precipitate was isolated by centrifugation and washed by acetone. The reaction yield was 186 mg, which corresponds to 88% for $y = 2$.

Preparation of Nanosized $[(\text{Mo}_6\text{I}_8)(\text{H}_2\text{O})_2(\text{OH})_4]\cdot y\text{H}_2\text{O}$ (nAH). A total of 300 mg of $(\text{Bu}_4\text{N})_2[(\text{Mo}_6\text{I}_8)(\text{NO}_3)_6]$ was dissolved in acetone (100 mL) containing some moisture, and the solution was left to stand. After 1 week, the solution had become opalescent, indicating the formation of nanoparticles. After 2 months, a precipitate had formed because of hydrolysis of the starting complex, was isolated by centrifugation, washed with acetone three times, and then dried in air at 50 °C to constant mass. The reaction yield after 2 months was 30 mg, which corresponds to 14% for $y = 2$.

Photocatalytic Experiments. In a typical photocatalytic test, 20 mg of sample was placed in a quartz reactor, 80 mL of water was added, and the mixture was ultrasonicated for 5 min. Then organic dye RhB was added to achieve the concentration of 2.5 mg L⁻¹. The mixture in the reactor was vigorously stirred in darkness for 2 h to reach adsorption–desorption equilibrium. After that, a probe (8 mL) was collected, and the remaining solution was irradiated with UV (365 ± 5 nm) or visible (~400–700 nm) light. The distance between the reactor and light source was 10 mm. At regular intervals of irradiation time, probes were collected (5, 15, 30, 45, 60, 75, 90, 105, 120, 180, and 300 min) and centrifuged. UV–vis spectra of the isolated solutions were recorded in order to estimate the concentration of RhB. The decrease of the RhB concentration was tracked by its characteristic optical absorbance at 554 nm.

In order to verify the stability of the photocatalysts and their ability to be used repeatedly, we carried out recycling experiments. At the end of each run (60 min of irradiation), after the UV–vis spectrum was recorded, the precipitate was placed back into the reaction mixture and the initial concentration of RhB (2.5 mg/L) and volume of the mixture (80 mL) were adjusted by the addition of a RhB solution.

To shed light on the mechanism of photocatalysis, scavengers for ROS and other active species were used: ammonium oxalate for holes, ascorbic acid for superoxide anion radicals and singlet oxygen, and ethanol for hydroxyl radicals. A 1 mmol L⁻¹ scavenger was added to the reaction mixture during the typical photocatalytic experiment, and its effect on the RhB degradation was monitored.

RESULTS AND DISCUSSION

Synthesis and Characterization of Materials. Octahedral molybdenum cluster complexes possess interesting properties, particularly, ROS generation.^{13,14,20–23} This property can be used to develop new cluster-based photocatalysts for the removal of organic pollutants from wastewater. However, to stabilize the catalytically active centers, facilitate the separation of the material used, and improve its functional characteristics, it is of practical interest to develop new hybrid or composite materials with molybdenum clusters and an appropriate matrix. h-BN seems to be very perspective in such a role because of its high thermal and chemical stability, transparency in the visible and near-UV range, and ability to effectively separate charge carriers, preventing their recombination. However, h-BN in its original form is a chemically inert, hydrophobic, and low-surface-area material. For use in composites, these issues may be successfully overcome by surface functionalization, exfoliation, and the addition of potential anchoring sites. Therefore, for cluster immobilization, we used h-BN pretreated by H₂O₂ in an autoclave at 80 °C following our previously developed method.⁵¹ This procedure gives exfoliated BNNS with thicknesses of up to several layers and average lateral sizes of 200–600 nm (Figure S2A,B,D),

retaining the h-BN crystal structure (Figure S3, line A). H₂O₂ treatment functionalizes the h-BN surface with hydrophilic –OH groups and other defects,⁵¹ rendering the product dispersible in water (Figure S2C) and assisting the anchoring of molybdenum clusters.

First, the BNNS sample was impregnated with an acetone solution of $(\text{Bu}_4\text{N})_2[(\text{Mo}_6\text{I}_8)\text{I}_6]$ under a constant ultrasonic treatment to achieve better matrix exfoliation. The solid phase of the mixture was thoroughly washed to remove the unsupported cluster complex. The obtained sample had a white color, as well as BNNS, while the initial cluster was dark-red, thus indicating a low degree of the cluster inclusion. The molybdenum content in the sample was less than 0.1 wt % according to ICP-AES. Thus, impregnation of the matrix with a $(\text{Bu}_4\text{N})_2[(\text{Mo}_6\text{I}_8)\text{I}_6]$ solution did not lead to the anchoring of a significant amount of the cluster. Apparently, in this system, no notable interactions between cluster complex and BNNS occur because of the strong bonding between the cluster core and apical iodine ligand.

Therefore, we decided to utilize cluster complexes with labile ligands, enabling potentially advantageous chemical transformations. Our broad experience in cluster science has led our attention to the hydrolysis of clusters with labile ligands, producing an insoluble aqua–hydroxo complex, $[(\text{Mo}_6\text{I}_8)(\text{H}_2\text{O})_2(\text{OH})_4]\cdot y\text{H}_2\text{O}$ (AH).^{7,9,14,52–54} Therefore, to fabricate the h-BN/cluster nanocomposites, we designed and experimentally tested a special one-pot process featuring the in situ hydrolysis of $(\text{Bu}_4\text{N})_2[(\text{Mo}_6\text{I}_8)(\text{NO}_3)_6]$ with a labile NO₃⁻ ligand during BNNS impregnation. Taking into account the synthetic conditions, we can suggest that the parent cluster transforms into insoluble AH. By variation of the initial mixture composition, a series of samples AH_x/BNNS were obtained (x is the moles of the cluster $(\text{Bu}_4\text{N})_2[(\text{Mo}_6\text{I}_8)(\text{NO}_3)_6]$ on 1 mol of BNNS). The orange color of the resulting samples indicates the successful inclusion of a cluster complex. The molybdenum content found by ICP-AES in the composite depends on the initial component ratio in the synthetic mixture, as illustrated in Figure 2.

Up to $x = 0.03$, the molybdenum content in the samples rises linearly with an increase of the cluster concentration in

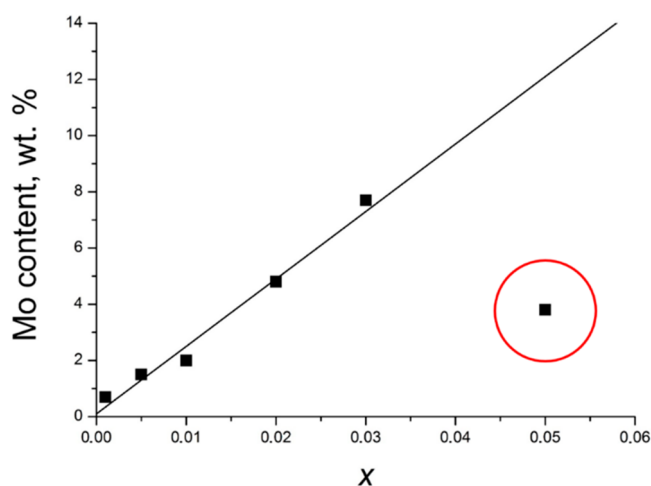


Figure 2. ICP-AES data on the molybdenum content in the AH_x/BNNS versus component ratio (x is the moles of $(\text{Bu}_4\text{N})_2[(\text{Mo}_6\text{I}_8)(\text{NO}_3)_6]$ to 1 mol of BNNS). The line is an approximation of the data (for x from 0.005 to 0.03).

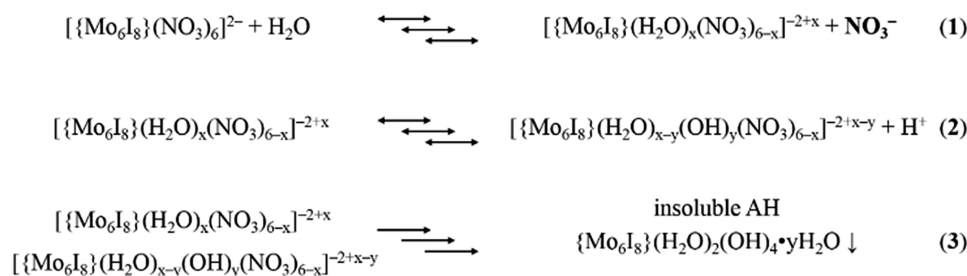


Figure 3. Simplified process of $(\text{Bu}_4\text{N})_2[\{\text{Mo}_6\text{I}_8\}(\text{NO}_3)_6]$ hydrolysis in water-containing media described as parallel steps: (1) substitution of NO_3^- ligands with water molecules (the release of free NO_3^- groups should be taken into account); (2) removal of protons from coordinated water, resulting in coordinated OH^- ; (3) transformation of soluble forms [reactions (1) and (2)] into the insoluble AH compound.

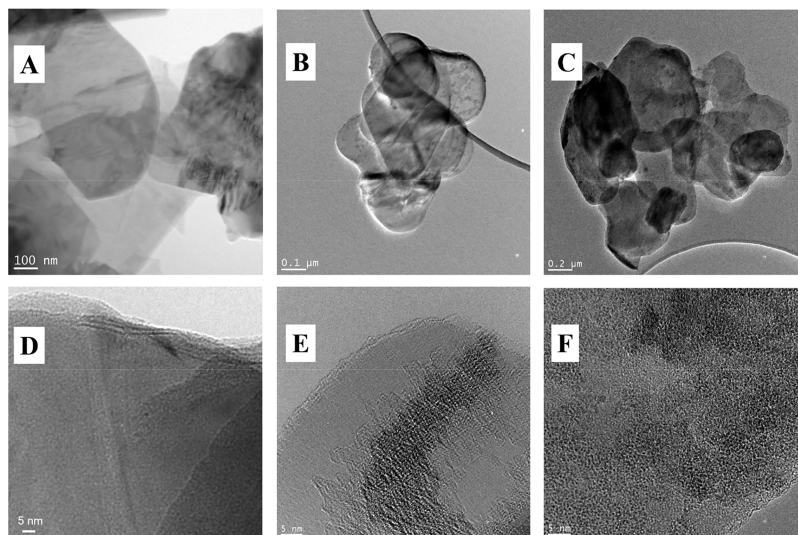


Figure 4. TEM/HRTEM images of the samples BNNS (A and D), $\text{AH}_{0.01}/\text{BNNS}$ (B and E), and $\text{AH}_{0.05}/\text{BNNS}$ (C and F).

the initial mixture. However, at $x = 0.05$, a sharp decrease in the molybdenum content is observed, which indicates a lower yield of the insoluble AH. This effect is well reproducible and seems to be due to both kinetic and thermodynamic reasons. Hydrolysis of $(\text{Bu}_4\text{N})_2[\{\text{Mo}_6\text{I}_8\}(\text{NO}_3)_6]$ in solution is a complicated and pH-dependent multistep process (Figure 3).⁹ It starts with the substitution of NO_3^- ligands with water molecules (reaction 1), followed by water deprotonation (reaction 2), which can occur in parallel. It seems that the first stages of the hydrolysis (1) and (2) in Figure 3 proceed fast and produce many soluble partially substituted forms. After some time, various forms can be found in the solution experimentally,⁹ which ultimately transform into nonsoluble AH ($[\{\text{Mo}_6\text{I}_8\}(\text{H}_2\text{O})_2(\text{OH})_4] \cdot y\text{H}_2\text{O}$) [reaction (3)]. At high $(\text{Bu}_4\text{N})_2[\{\text{Mo}_6\text{I}_8\}(\text{NO}_3)_6]$ concentration ($x = 0.05$), the final steps of hydrolysis (3) are inhibited. To explain this phenomenon, we can put forward two assumptions. First, it can be due to a lowered water concentration in the mixture. In our experiments, a water admixture, which is essential for hydrolysis processes, was being wasted as a ligand in reaction (1) and coprecipitated with AH in reaction (3). Second, AH precipitation leads to an increase in the free NO_3^- concentration relative to the total cluster complex concentration in solution, thereby shifting the equilibrium of reaction (1) to the left. A similar behavior was shown in our previous work⁷ on a related cluster complex $[\{\text{Mo}_6\text{I}_8\}(\text{DMSO})_6]^{4+}$ with another labile ligand, namely, dimethyl sulfoxide (DMSO); i.e.,

an increase of the DMSO concentration in solution resulted in a decrease of the hydrolysis rate.

Additional data on the composition as well as on the morphology of the samples were obtained by TEM/EDS (Figure 4). In the case of samples with clusters, the observed particle sizes of around several hundred nanometers (Figure 4B,C) well correspond to the size of BNNS (Figure 4A, D). It is clearly seen in HRTEM images (Figure 4E,F) that the BNNS surface is decorated by a thin film, containing Mo and I atoms, as proven by elemental mapping (Figures S4C,F,G and S5C,F,G). This film is probably amorphous because powder XRD patterns show only reflexes from well-crystalline h-BN even for the highest molybdenum content (Figure S3, lines B and C). In the $\text{AH}_{0.01}/\text{BNNS}$ composite, there are areas of free h-BN surface because the molybdenum content is relatively low (Figures 4B,E and S4). On the other hand, in $\text{AH}_{0.05}/\text{BNNS}$, when the molybdenum content is higher, most of the BNNS surface is covered by a cluster-containing amorphous phase (Figures 4C,F and S5).

To shed light on the possible mechanism and to obtain a clue to the role of the colloidal BNNS support in the formation and attachment of the AH compound, we prepared an unsupported AH cluster complex under conditions very close to those used for composites AH_x/BNNS (Figure S6). The TEM images show that the sample contains particles of 30–50 nm size (nanosized sample referred to as nAH), which are amorphous according to the electron diffraction image (Figure S6B) and XRD (Figure S7). The AH phase on the surface of

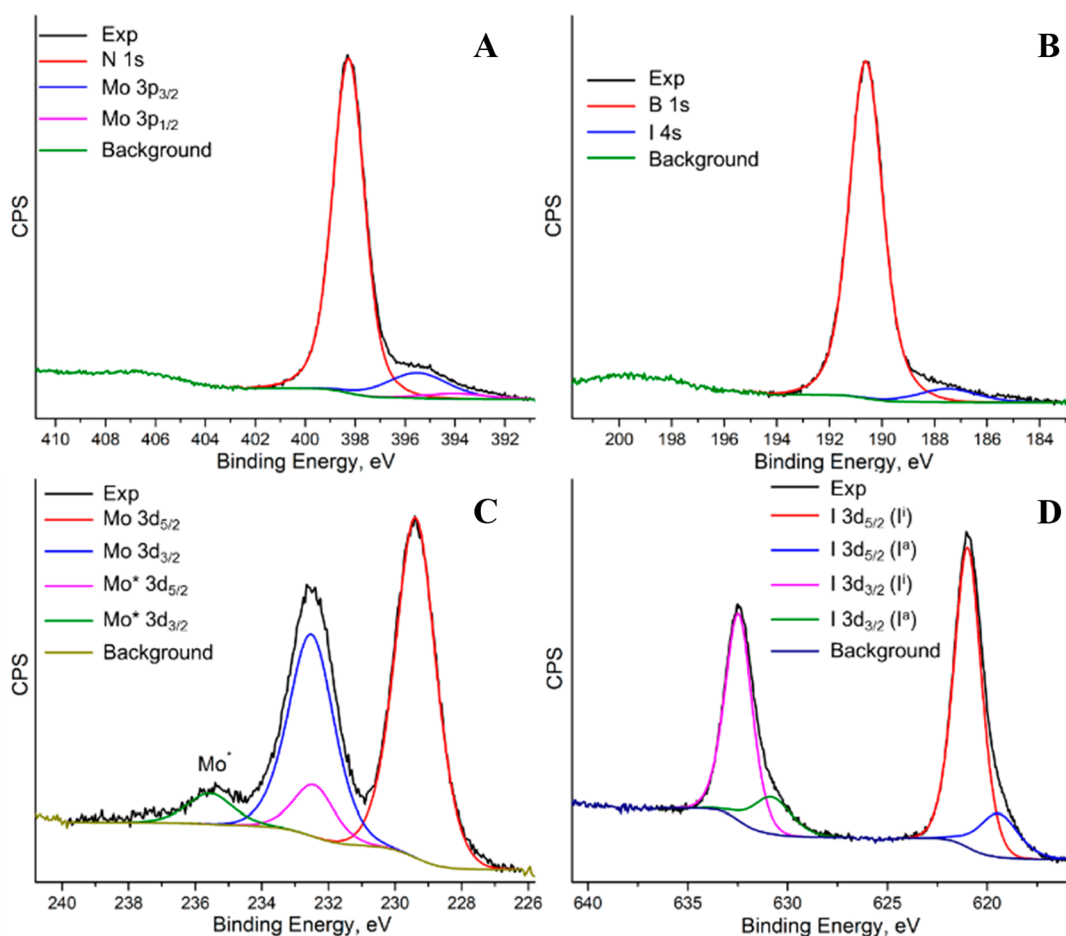


Figure 5. XPS spectra showing the N 1s (A), B 1s (B), Mo 3d (C), and I 3d (D) core levels in the $\text{AH}_{0.05}/\text{BNNS}$ composite.

BNNS is also amorphous but exists in the form of a continuous thin film (Figure 4E,F). Different morphologies of free and deposited AH phases indicate the important role of the BNNS support in AH formation. Overall, AH growth in the presence of the hydrophilic support BNNS preferably in the form of an extended thin film may proceed around active centers. Probably, partially hydrolyzed cluster forms coordinate to surface edges, defects, and functional groups.

AH_x/BNNS and reference samples [the initial BNNS and unsupported bulk AH (bAH)] were studied using XPS. The spectrum of the initial BNNS shows characteristic boron (B 1s, 190.84 eV) and nitrogen (N 1s, 398.74 eV) peaks and a small amount of surface oxygen (Figure S8). After cluster deposition, the BNNS composition remains unchanged; however, as expected, the survey spectrum shows the appearance of new cluster-related peaks, namely, Mo 3d_{3/2} (232.5 eV), Mo 3d_{5/2} (229.2 eV), I 3d_{3/2} (632.5 eV), and I 3d_{5/2} (621 eV), which proves composite formation (typical spectra of the composites are shown in Figures 5 and S9). The molybdenum and iodine peak positions correlate perfectly with literature data for octahedral molybdenum iodide clusters and cluster-containing materials.^{55,56} Figure 5D demonstrates two additional shoulders at lower binding energies (619.5 and 630.8 eV) near the main peaks of the inner iodine ligands (I^b), which correspond to some unreacted apical ligands (I^a). This fact indicates that not all apical iodine ligands were replaced by NO₃⁻ during the cluster precursor preparation. Regarding the region of the Mo 3d core level, besides the main doublet of Mo

3d_{3/2} and Mo 3d_{5/2}, additional low-intensity doublet (peaks at 235.6 and 232.4 eV) was observed (Figure 5C). These peaks are probably due to slight cluster oxidation to the Mo^{VI} state under ultrasonication because in nonsonicated bAH only Mo^{II} atoms were found (Figure S10). Also, in the AH_x/BNNS spectra, only N atoms related to h-BN were observed (Figure 5A), indicating the complete removal of NO₃⁻ groups during in situ hydrolysis of the cluster precursor. Therefore, XPS does not reveal any specific interactions between the cluster complex and h-BN, suggesting deposition without chemical bond formation.

Cluster complex deposition on the surface of BNNS leads to a change in the sample color to orange; therefore, we decided to investigate their optical properties. The recorded diffuse-reflectance spectra of AH_x/BNNS composites and both individual compounds (BNNS and bAH) were converted to absorption spectra using the Kubelka–Munk function (Figure S11A). Data obtained show that individual BNNS have no absorption in the studied region (250–800 nm). For composite materials, an absorption band is observed up to 700 nm. It should be noted that the profiles of the absorption spectra of the nanocomposite materials and bAH are similar, which further confirms cluster complex deposition on the BNNS surface in the AH form. To measure the band gap (E_g) of the materials, the Tauc plot method was used (Figure S11B). The E_g value of the initial BNNS lies outside the limits of the studied region and exceeds 5 eV.⁵⁷ The E_g value for bAH was estimated to be ~1.7 eV. For the composites $\text{AH}_{0.03}/$

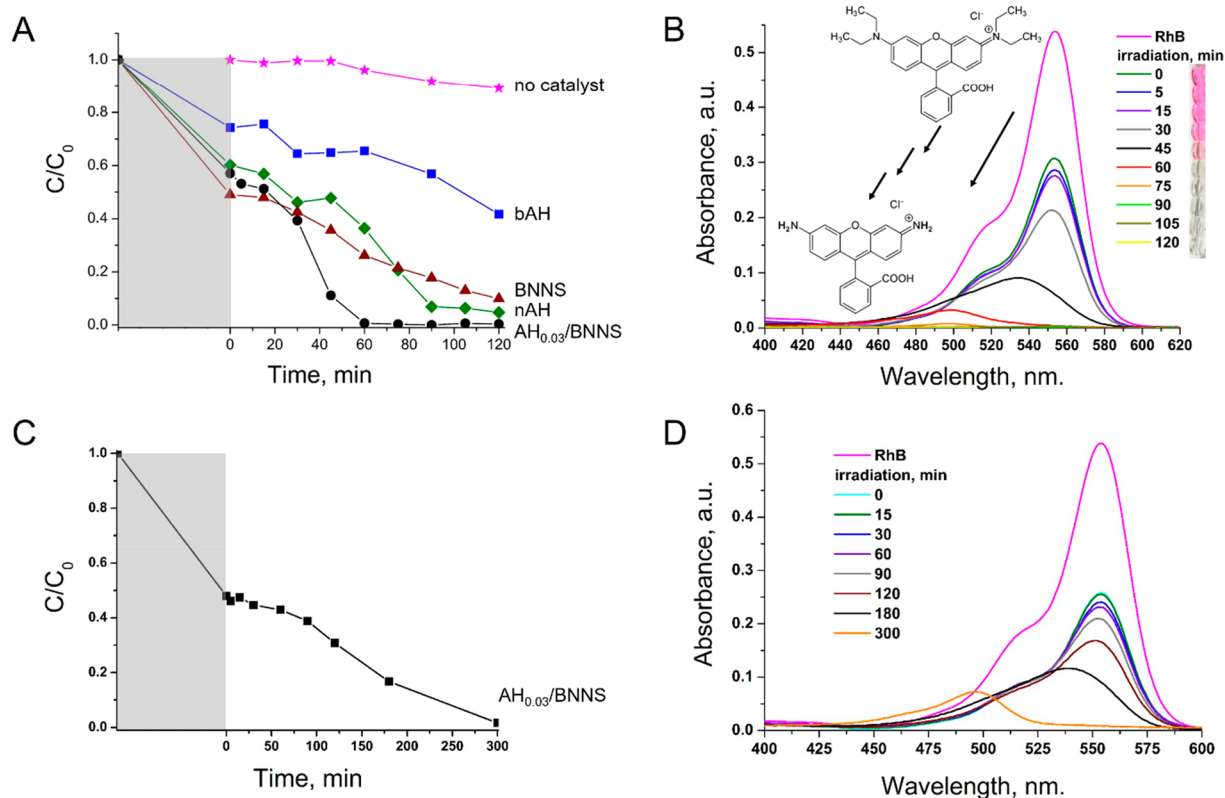


Figure 6. (A) C/C_0 ratio versus irradiation time for the photocatalytic decomposition of RhB under UV light (365 ± 5 nm): blank experiment without any catalyst; photocatalytic degradation on the bAH, BNNS, nAH, and $AH_{0.03}/BNNS$ (top-down). (B) UV-vis spectra of a RhB solution before and after irradiation during different time intervals (up to 120 min) in the presence of $AH_{0.03}/BNNS$. The insets are structures of RhB and intermediate degradation product (deethylated form) (up) and solution photographs (down). (C) C/C_0 versus irradiation time for the photocatalytic decomposition of RhB in the presence of $AH_{0.03}/BNNS$ under visible light. (D) UV-vis spectra of a RhB solution before and after irradiation during different time intervals (up to 300 min) in the presence of $AH_{0.03}/BNNS$. Gray areas show the 2 h sorption stages.

BNNS and $AH_{0.05}/BNNS$, the values were close to that of the unsupported bAH. Overall, cluster deposition results in the appearance of absorption in the visible region, leading us to study the $AH_x/BNNS$ photocatalytic properties.

Photocatalytic Properties of Materials. The $AH_x/BNNS$ samples were tested as photocatalytic materials in the degradation of RhB as a model organic pollutant (Figure 6). Because the aqueous solution of RhB has an absorption maximum at 554 nm, a decrease in the intensity of this absorption band was used to monitor the decomposition process. RhB is quite stable under UV-light irradiation (the decomposition degree is less than 10% after 120 min; Figure 6A). Before the photodegradation study, a mixture of dye and photocatalyst was stirred for 2 h in the dark to achieve sorption-desorption equilibrium (Figure S12).⁵⁸ Figure 6A shows the values of C/C_0 of RhB after the sorption stage (0 min of irradiation) and after different time intervals of irradiation of BNNS and various samples: bAH, nAH, and composite $AH_{0.03}/BNNS$. In the cases of individual components (BNNS, bAH, and nAH), decomposition proceeds much better than that in the blank experiment without any catalyst (Figure 6A), but the reaction was not completed even in 120 min. It should be noted that the nanosized form of AH (nAH) has better photocatalytic properties than the bulk one (bAH). At the same time, the composites $AH_x/BNNS$ show the best properties, making the RhB solution colorless after UV-light irradiation for 60–90 min. The better performance of the

composites appears to be caused by the coaction of both components, and BNNS acts not simply as a carrier but also as a cocatalyst.^{2,41–45} Along with a decrease in dye absorption, bands related to the consecutive formation of deethylated RhB forms appear at 500–540 nm (Figure 6B). RhB deethylation is typical for photocatalysts based on molybdenum clusters^{20,21} and many other materials.^{2,59,60} When irradiation is prolonged, these bands also finally lose their intensity, indicating further decomposition (Figure 6B).

The best activity was demonstrated by $AH_{0.03}/BNNS$ (Figures S13 and S14) probably because of the highest amount of cluster and, therefore, increased coating of BNNS by the AH film. The value of the reaction rate constant (pseudo-first-order reaction) for $AH_{0.03}/BNNS$ was estimated as 0.013 min^{-1} (Figure S15). It is worth noting that the reaction rate depends on many parameters, including the dye and catalyst concentrations and lamp power, so a comparison with other catalysts is rather qualitative, especially taking into account that this work is one of a few studying the photocatalytic dye decomposition on hexamolybdenum clusters.^{20,21} Overall, the obtained constant value is close to those of other promising heterogeneous photocatalysts in the RhB degradation process.^{2,61}

The prolonged activity and stability of the materials $AH_{0.03}/BNNS$ were investigated by cycling experiments (Figures 7 and S16). As was mentioned above, complete RhB degradation with $AH_{0.03}/BNNS$ requires 60 min of irradiation. After each

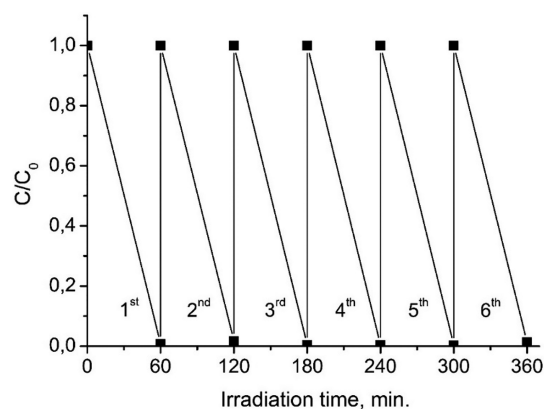


Figure 7. Cycling of $\text{AH}_{0.03}/\text{BNNS}$ in RhB photocatalytic decomposition.

run, the initial concentration of RhB and the volume of the mixture were readjusted. The resulting material retains its efficiency at least for six cycles. The good stability during the photocatalytic reactions is probably related to several factors, such as (i) insolubility of the AH cluster, (ii) effective stabilization of the cluster phase on surface defects or/and functional groups, and (iii) photocatalytic mechanism, which does not include active site dissolution (see below).

As shown earlier, cluster deposition led to an increase in AH_x/BNNS light absorption in the visible region; therefore, we further studied the photocatalytic properties utilizing an IKEA table lamp, emitting in the range of $\sim 400\text{--}700\text{ nm}$ (Figure S1). RhB completely decomposes in the presence of a $\text{AH}_{0.03}/\text{BNNS}$ composite, although it takes somewhat longer than under UV irradiation (Figure 6C,D). The degradation proceeds through the formation of intermediate deethylated forms, similar to the case of UV irradiation. This experiment is very important for further practical applications in sunlight-driven photocatalytic water purification. Because the sunlight spectrum contains both UV and visible components, a higher efficiency of the catalysts is expected.

Study of the Photocatalytic Mechanism. Apparently, RhB decomposition is a complex photocatalytic process that causes nonideal shapes of the curves (Figure 6). The overall mechanism may be imagined as schematically drawn in Figure 8. The absorption of a light quantum leads to the transition of the cluster fragment to the long-lived excited state, producing an electron–hole pair. Both active species can be separated by diffusion to the AH film surface; however, their unfavorable recombination may occur, leading to a decrease in the excited-

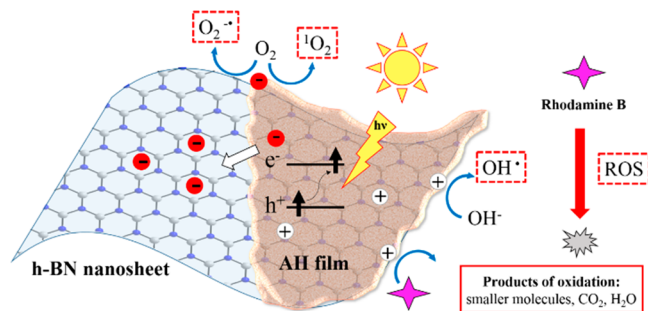


Figure 8. Schematic of the photocatalytic process of organic dye decomposition in the presence of composite AH/BNNS . AH is $[\{\text{Mo}_6\text{I}_8\}(\text{H}_2\text{O})_2(\text{OH})_4] \cdot y\text{H}_2\text{O}$.

state quantum yield. Recombination effects may be somewhat diminished by the h-BN support because it favors charge separation.^{2,46,62} Surface holes can also react with hydroxide ions to form a highly active hydroxyl radical (OH^\bullet), while surface electrons convert molecular oxygen dissolved in the system into superoxide radicals ($\text{O}_2^{\bullet-}$). In addition, molybdenum cluster complexes are well-known for their efficiency in the generation of singlet oxygen ($^1\text{O}_2$).^{11,13,14,23} All of these highly reactive species can oxidize dye molecules dissolved in water, leading to their destruction and ultimate mineralization of the mixture.^{20,21,46}

To gain insight into the role of different potential active species in our photocatalytic process, we conducted trapping experiments with ascorbic acid ($\text{O}_2^{\bullet-}$ and $^1\text{O}_2$ scavenger),⁶³ ethanol (OH^\bullet scavenger),⁶⁴ and ammonium oxalate (h^+ scavenger).⁶⁵ A photocatalytic activity drop in the presence of a certain scavenger indicates that the target species has an active part in the process.^{4–6} As follows from Figure 9, only ascorbic acid is capable of preventing complete RhB degradation, thus indicating that $\text{O}_2^{\bullet-}/^1\text{O}_2$ as probable photocatalytically active species.

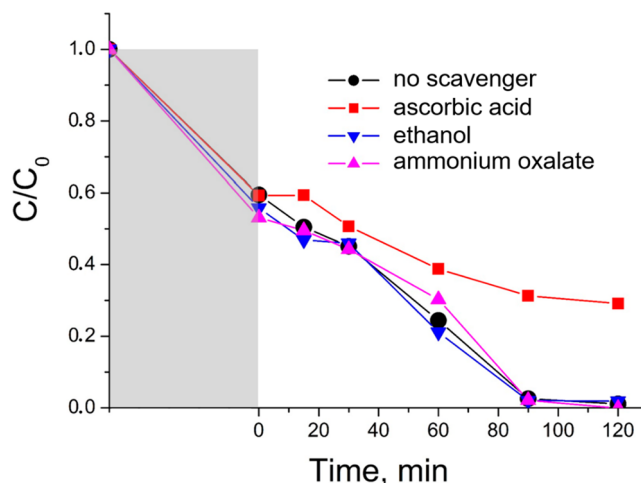


Figure 9. C/C_0 ratio versus irradiation time for photocatalytic RhB decomposition on $\text{AH}_{0.03}/\text{BNNS}$ under UV light: without any scavenger and in the presence of ascorbic acid, ethanol, and ammonium oxalate. The gray area shows the 2 h sorption stage.

Although superoxide radical formation by $[\{\text{Mo}_6\text{X}_8\}\text{L}_6]$ cluster complexes is unfavorable,²³ we suppose that $\text{O}_2^{\bullet-}$ may still be involved in the photocatalytic process because h-BN is able to stabilize electrons^{2,46,62} and generate $\text{O}_2^{\bullet-}$ itself.^{2,66} At the same time, cluster complexes produce $^1\text{O}_2$ well.^{11,13,14,23} These observations once again indicate that both components of the AH/BNNS catalyst participate in the photocatalytic process.

CONCLUSION

The present study demonstrates the deposition of hexamolybdenum cluster complexes onto hydrophilic functionalized h-BN nanosheets. The key to a successful immobilization was the use of a soluble precursor cluster with labile apical ligands ($\text{Bu}_4\text{N}\}_2[\{\text{Mo}_6\text{I}_8\}(\text{NO}_3)_6]$) able to undergo in situ hydrolysis resulting in formation of the insoluble $[\{\text{Mo}_6\text{I}_8\}(\text{H}_2\text{O})_2(\text{OH})_4] \cdot y\text{H}_2\text{O}$ on a modified h-BN nanosheet surface as a thin amorphous film. The reaction of RhB degradation as a modeling wastewater purification was used to demonstrate the

practical potential of the designed catalyst. In contrast to individual h-BN nanosheets and cluster complexes, nanocomposites exhibited full decomposition of the dye under both UV and visible light, retaining their activity for at least six cycles. Scavenger experiments reveal the important contribution of the $O_2^{\bullet-}$ and 1O_2 to the photocatalytic process. A better performance of composite materials appears to be caused by the coaction of both components: (i) cluster complexes have high absorption in the visible region and noticeable photocatalytic properties; (ii) h-BN stabilizes the active phase in thin-film morphology, possibly enhancing dye sorption, benefits effective charge-carrier separation, and even manifests its own additional catalytic activity. Overall, this study evidences that molybdenum cluster complexes are promising candidates to obtain nanocomposites with advanced characteristics and opens up rich possibilities for future research directed at the catalytic elimination of pollutants, ecofriendly catalysts, and other areas related to environmental protection.

■ ASSOCIATED CONTENT

SI Supporting Information

The Supporting Information is available free of charge at <https://pubs.acs.org/doi/10.1021/acs.inorgchem.0c00528>.

LED lamp spectrum, HRTEM, EDS, XRD, XPS, diffuse-reflectance spectra, sorption of RhB, UV–vis spectra of RhB solutions, kinetic study, and cycling experiments (PDF)

■ AUTHOR INFORMATION

Corresponding Authors

Mariia N. Ivanova – Nikolaev Institute of Inorganic Chemistry, Siberian Branch of the Russian Academy of Sciences, 630090 Novosibirsk, Russian Federation; orcid.org/0000-0001-5798-7211; Phone: +73833309253; Email: kozlova@niic.nsc.ru; Fax: +73833309489

Ekaterina D. Grayfer – Nikolaev Institute of Inorganic Chemistry, Siberian Branch of the Russian Academy of Sciences, 630090 Novosibirsk, Russian Federation; orcid.org/0000-0002-2994-959X; Phone: +73833309253; Email: grayfer@niic.nsc.ru; Fax: +73833309489

Authors

Yuri A. Vorotnikov – Nikolaev Institute of Inorganic Chemistry, Siberian Branch of the Russian Academy of Sciences, 630090 Novosibirsk, Russian Federation; orcid.org/0000-0002-7807-4697

Elena E. Plotnikova – Nikolaev Institute of Inorganic Chemistry, Siberian Branch of the Russian Academy of Sciences, 630090 Novosibirsk, Russian Federation

Margarita V. Marchuk – Nikolaev Institute of Inorganic Chemistry, Siberian Branch of the Russian Academy of Sciences, 630090 Novosibirsk, Russian Federation

Anton A. Ivanov – Nikolaev Institute of Inorganic Chemistry, Siberian Branch of the Russian Academy of Sciences, 630090 Novosibirsk, Russian Federation; orcid.org/0000-0003-2026-8568

Igor P. Asanov – Nikolaev Institute of Inorganic Chemistry, Siberian Branch of the Russian Academy of Sciences, 630090 Novosibirsk, Russian Federation

Alphiya R. Tsygankova – Nikolaev Institute of Inorganic Chemistry, Siberian Branch of the Russian Academy of Sciences, 630090 Novosibirsk, Russian Federation

Vladimir E. Fedorov – Nikolaev Institute of Inorganic Chemistry, Siberian Branch of the Russian Academy of Sciences, 630090 Novosibirsk, Russian Federation

Michael A. Shestopalov – Nikolaev Institute of Inorganic Chemistry, Siberian Branch of the Russian Academy of Sciences, 630090 Novosibirsk, Russian Federation; orcid.org/0000-0001-9833-6060

Complete contact information is available at:

<https://pubs.acs.org/10.1021/acs.inorgchem.0c00528>

Author Contributions

The manuscript was written through contributions of all authors. All authors have given approval to the final version of the manuscript.

Notes

The authors declare no competing financial interest.

■ ACKNOWLEDGMENTS

The work was supported by the Russian Foundation for Basic Research (Grant 17-03-00140). E.D.G. and M.N.I. thank the President of the Russian Federation for scholarship awards (CII-140.2018.1 and CII-3729.2019.1, respectively).

■ REFERENCES

- (1) Muhd Julkapli, N.; Bagheri, S.; Bee Abd Hamid, S. B. Recent Advances in Heterogeneous Photocatalytic Decolorization of Synthetic Dyes. *Sci. World J.* **2014**, *2014*, 1.
- (2) Zhou, C. Y.; Lai, C.; Zhang, C.; Zeng, G. M.; Huang, D. L.; Cheng, M.; Hu, L.; Xiong, W. P.; Chen, M.; Wang, J. J.; Yang, Y.; Jiang, L. B. Semiconductor/Boron Nitride Composites: Synthesis, Properties, and Photocatalysis Applications. *Appl. Catal., B* **2018**, *238*, 6–18.
- (3) Schneider, J.; Matsuoka, M.; Takeuchi, M.; Zhang, J.; Horiuchi, Y.; Anpo, M.; Bahnemann, D. W. Understanding TiO₂ Photocatalysis: Mechanisms and Materials. *Chem. Rev.* **2014**, *114* (19), 9919–9986.
- (4) Wang, X.; Zhang, S.; Song, S.; Gu, P.; Ma, R.; Wei, D.; Zhao, G.; Wen, T.; Jehan, R.; Hu, B. Visible-light-driven activation of persulfate over cyano and hydroxyl groups co-modified mesoporous g-C₃N₄ for boosting bisphenol A degradation. *J. Mater. Chem. A* **2019**, *7*, 5552–5560.
- (5) Zhao, G.; Sun, Y.; Zhao, Y.; Wen, T.; Wang, X.; Chen, Z.; Sheng, G.; Chen, C.; Wang, X. Enhanced photocatalytic simultaneous removals of Cr (VI) and bisphenol A over Co (II)-modified TiO₂. *Langmuir* **2019**, *35* (1), 276–283.
- (6) Wang, H.; Zhang, N.; Cheng, G.; Guo, H.; Shen, Z.; Yang, L.; Zhao, Y.; Alsaedi, A.; Hayat, T.; Wang, X. Preparing a photocatalytic Fe doped TiO₂/rGO for enhanced bisphenol A and its analogues degradation in water sample. *Appl. Surf. Sci.* **2020**, *505*, 144640.
- (7) Svezhentseva, E. V.; Vorotnikov, Y. A.; Solovieva, A. O.; Pozmogova, T. N.; Eltsov, I. V.; Ivanov, A. A.; Evtushok, D. V.; Miroshnichenko, S. M.; Yanshole, V. V.; Eling, C. J.; Adawi, A. M.; Bouillard, J. S. G.; Kuratieva, N. V.; Fufaeva, M. S.; Shestopalova, L. V.; Mironov, Y. V.; Efremova, O. A.; Shestopalov, M. A. From Photoinduced to Dark Cytotoxicity through an Octahedral Cluster Hydrolysis. *Chem. - Eur. J.* **2018**, *24* (68), 17915–17920.
- (8) Vorotnikova, N. A.; Edeleva, M. V.; Kurskaya, O. G.; Brylev, K. A.; Shestopalov, A. M.; Mironov, Y. V.; Sutherland, A. J.; Efremova, O. A.; Shestopalov, M. A. One-pot Synthesis of {Mo₆I₈}⁴⁺-doped Polystyrene Microspheres via a Free Radical Dispersion Copolymerisation Reaction. *Polym. Int.* **2017**, *66* (12), 1906–1912.
- (9) Cheplakova, A. M.; Solovieva, A. O.; Pozmogova, T. N.; Vorotnikov, Y. A.; Brylev, K. A.; Vorotnikova, N. A.; Vorontsova, E. V.; Mironov, Y. V.; Poveshchenko, A. F.; Kovalenko, K. A.; Shestopalov, M. A. Nanosized Mesoporous Metal-organic Framework MIL-101 as a Nanocarrier for Photoactive Hexamolybdenum Cluster Compounds. *J. Inorg. Biochem.* **2017**, *166*, 100–107.

- (10) Vorotnikova, N. A.; Efremova, O. A.; Tsygankova, A. R.; Brylev, K. A.; Edeleva, M. V.; Kurskaya, O. G.; Sutherland, A. J.; Shestopalov, M. A.; Mironov, Y. V.; Shestopalov, M. A. Characterization and Cytotoxicity Studies of Thiol-modified Polystyrene Microbeads Doped with $[\{\text{Mo}_6\text{X}_8\}(\text{NO}_3)_6]^{2-}$ ($\text{X} = \text{Cl}, \text{Br}, \text{I}$). *Polym. Adv. Technol.* **2016**, *27* (7), 922–928.
- (11) Efremova, O. A.; Vorotnikov, Y. A.; Brylev, K. A.; Vorotnikova, N. A.; Novozhilov, I. N.; Kuratieva, N. V.; Edeleva, M. V.; Benoit, D. M.; Kitamura, N.; Mironov, Y. V.; Shestopalov, M. A.; Sutherland, A. J. Octahedral molybdenum cluster complexes with aromatic sulfonate ligands. *Dalton Trans.* **2016**, *45* (39), 15427–15435.
- (12) Efremova, O. A.; Brylev, K. A.; Vorotnikov, Y. A.; Vejsadova, L.; Shestopalov, M. A.; Chimionides, G. F.; Mikes, P.; Topham, P. D.; Kim, S. J.; Kitamura, N.; Sutherland, A. J. Photoluminescent Materials Based on PMMA and a Highly-emissive Octahedral Molybdenum Metal Cluster Complex. *J. Mater. Chem. C* **2016**, *4* (3), 497–503.
- (13) Solovieva, A. O.; Vorotnikov, Y. A.; Trifonova, K. E.; Efremova, O. A.; Krasnikova, A. A.; Brylev, K. A.; Vorontsova, E. V.; Avrorov, P. A.; Shestopalova, L. V.; Poveshchenko, A. F.; Mironov, Y. V.; Shestopalov, M. A. Cellular internalisation, bioimaging and dark and photodynamic cytotoxicity of silica nanoparticles doped by $\{\text{Mo}_6\text{I}_8\}^{4+}$ metal clusters. *J. Mater. Chem. B* **2016**, *4* (28), 4839–4846.
- (14) Vorotnikov, Y. A.; Efremova, O. A.; Vorotnikova, N. A.; Brylev, K. A.; Edeleva, M. V.; Tsygankova, A. R.; Smolentsev, A. I.; Kitamura, N.; Mironov, Y. V.; Shestopalov, M. A. On the Synthesis and Characterisation of Luminescent Hybrid Particles: Mo_6 Metal Cluster Complex/ SiO_2 . *RSC Adv.* **2016**, *6* (49), 43367–43375.
- (15) Vorotnikov, Y. A.; Pozmogova, T. N.; Solovieva, A. O.; Miroshnichenko, S. M.; Vorontsova, E. V.; Shestopalova, L. V.; Mironov, Y. V.; Shestopalov, M. A.; Efremova, O. A. Luminescent Silica Mesoparticles for Protein Transduction. *Mater. Sci. Eng., C* **2019**, *96*, 530–538.
- (16) Efremova, O. A.; Shestopalov, M. A.; Chirtsova, N. A.; Smolentsev, A. I.; Mironov, Y. V.; Kitamura, N.; Brylev, K. A.; Sutherland, A. J. A Highly Emissive Inorganic Hexamolybdenum Cluster Complex as a Handy Precursor for the Preparation of New Luminescent Materials. *Dalton Trans.* **2014**, *43* (16), 6021–6025.
- (17) Evtushok, D. V.; Melnikov, A. R.; Vorotnikova, N. A.; Vorotnikov, Y. A.; Ryadun, A. A.; Kuratieva, N. V.; Kozyr, K. V.; Obedinskaya, N. R.; Kretov, E. I.; Novozhilov, I. N.; Mironov, Y. V.; Stass, D. V.; Efremova, O. A.; Shestopalov, M. A. A Comparative Study of Optical Properties and X-ray Induced Luminescence of Octahedral Molybdenum and Tungsten Cluster Complexes. *Dalton Trans.* **2017**, *46* (35), 11738–11747.
- (18) Evtushok, D. V.; Vorotnikova, N. A.; Logvinenko, V. A.; Smolentsev, A. I.; Brylev, K. A.; Plyusnin, P. E.; Pishchur, D. P.; Kitamura, N.; Mironov, Y. V.; Solovieva, A. O.; Efremova, O. A.; Shestopalov, M. A. Luminescent coordination polymers based on Ca^{2+} and octahedral cluster anions $[\{\text{M}_6\text{Cl}_8\}\text{Cl}_6]^{12-}$ ($\text{M} = \text{Mo}, \text{W}$): synthesis and thermal stability studies. *New J. Chem.* **2017**, *41* (24), 14855–14861.
- (19) Sokolov, M. N.; Mihailov, M. A.; Peresyphina, E. V.; Brylev, K. A.; Kitamura, N.; Fedin, V. P. Highly Luminescent Complexes $[\text{Mo}_6\text{X}_8(\text{n-C}_3\text{F}_7\text{COO})_6]^{2-}$ ($\text{X} = \text{Br}, \text{I}$). *Dalton Trans.* **2011**, *40* (24), 6375–6377.
- (20) Barras, A.; Das, M. R.; Devarapalli, R. R.; Shelke, M. V.; Cordier, S.; Szunerits, S.; Boukherroub, R. One-pot Synthesis of Gold Nanoparticle/Molybdenum Cluster/Graphene Oxide Nanocomposite and Its Photocatalytic Activity. *Appl. Catal., B* **2013**, *130*, 270–276.
- (21) Barras, A.; Cordier, S.; Boukherroub, R. Fast Photocatalytic Degradation of Rhodamine B over $[\text{Mo}_6\text{Br}_8(\text{N}_3)_6]^{2-}$ Cluster Units under Sun Light Irradiation. *Appl. Catal., B* **2012**, *123*, 1–8.
- (22) Elistratova, J.; Mukhametshina, A.; Kholin, K.; Nizameev, I.; Mikhailov, M.; Sokolov, M.; Khairullin, R.; Miftakhova, R.; Shammas, G.; Kadirov, M.; Petrov, K.; Rizvanov, A.; Mustafina, A. Interfacial Uploading of Luminescent Hexamolybdenum Cluster Units onto Amino-Decorated Silica Nanoparticles as New Design of Nanomaterial for Cellular Imaging and Photodynamic Therapy. *J. Colloid Interface Sci.* **2019**, *538*, 387–396.
- (23) Jackson, J. A.; Turro, C.; Newsham, M. D.; Nocera, D. G. Oxygen Quenching of Electronically Excited Hexanuclear Molybdenum and Tungsten Halide Clusters. *J. Phys. Chem.* **1990**, *94* (11), 4500–4507.
- (24) Molard, Y. Clustomesogens: Liquid Crystalline Hybrid Nanomaterials Containing Functional Metal Nanoclusters. *Acc. Chem. Res.* **2016**, *49* (8), 1514–1523.
- (25) Zhao, Y.; Lunt, R. R. Transparent Luminescent Solar Concentrators for Large-Area Solar Windows Enabled by Massive Stokes-Shift Nanocluster Phosphors. *Adv. Energy. Mater.* **2013**, *3* (9), 1143–1148.
- (26) Beltran, A.; Mikhailov, M.; Sokolov, M. N.; Perez-Laguna, V.; Rezusta, A.; Revillo, M. J.; Galindo, F. A Photobleaching Resistant Polymer Supported Hexanuclear Molybdenum Iodide Cluster for Photocatalytic Oxygenations and Photodynamic Inactivation of Staphylococcus Aureus. *J. Mater. Chem. B* **2016**, *4* (36), 5975–5979.
- (27) Felip-Leon, C.; Arnau del Valle, C.; Perez-Laguna, V.; Isabel Millan-Lou, M.; Miravet, J. F.; Mikhailov, M.; Sokolov, M. N.; Rezusta-Lopez, A.; Galindo, F. Superior Performance of Macroporous Over Gel Type Polystyrene as a Support for the Development of Photo-bactericidal Materials. *J. Mater. Chem. B* **2017**, *5* (30), 6058–6064.
- (28) Neaime, C.; Amela-Cortes, M.; Grasset, F.; Molard, Y.; Cordier, S.; Dierre, B.; Mortier, M.; Takei, T.; Takahashi, K.; Haneda, H.; Verelst, M.; Lechevallier, S. Time-gated Luminescence Bioimaging with New Luminescent Nanocolloids Based on $[\text{Mo}_6\text{I}_8(\text{C}_2\text{F}_5\text{COO})_6]^{2-}$ Metal Atom Clusters. *Phys. Chem. Chem. Phys.* **2016**, *18* (43), 30166–30173.
- (29) Kumar, S.; Khatri, O. P.; Cordier, S.; Boukherroub, R.; Jain, S. L. Graphene Oxide Supported Molybdenum Cluster: First Heterogenized Homogeneous Catalyst for the Synthesis of Dimethylcarbonate from CO_2 and Methanol. *Chem. - Eur. J.* **2015**, *21* (8), 3488–3494.
- (30) Kumar, P.; Mungse, H. P.; Cordier, S.; Boukherroub, R.; Khatri, O. P.; Jain, S. L. Hexamolybdenum clusters supported on graphene oxide: visible-light induced photocatalytic reduction of carbon dioxide into methanol. *Carbon* **2015**, *94*, 91–100.
- (31) Bůžek, D.; Hynek, J.; Kučeráková, M.; Kirakci, K.; Demel, J.; Lang, K. Mo^{II} cluster complex-based coordination polymer as an efficient heterogeneous catalyst in the Suzuki–Miyaura coupling reaction. *Eur. J. Inorg. Chem.* **2016**, *2016* (28), 4668–4673.
- (32) Grasset, F.; Dorson, F.; Cordier, S.; Molard, Y.; Perrin, C.; Marie, A. M.; Sasaki, T.; Haneda, H.; Bando, Y.; Mortier, M. Water-in-oil Microemulsion Preparation and Characterization of $\text{Cs}_2[\text{Mo}_6\text{X}_{14}]\text{@SiO}_2$ Phosphor Nanoparticles Based on Transition Metal Clusters ($\text{X} = \text{Cl}, \text{Br}, \text{and I}$). *Adv. Mater.* **2008**, *20* (1), 143.
- (33) Aubert, T.; Cabello-Hurtado, F.; Esnault, M. A.; Neaime, C.; Le Bret-Chauvel, D.; Jeanne, S.; Pellen, P.; Roiland, C.; Le Polles, L.; Saito, N.; Kimoto, K.; Haneda, H.; Ohashi, N.; Grasset, F.; Cordier, S. Extended Investigations on Luminescent $\text{Cs}_2[\text{Mo}_6\text{Br}_{14}]\text{@SiO}_2$ Nanoparticles: Physico-Structural Characterizations and Toxicity Studies. *J. Phys. Chem. C* **2013**, *117* (39), 20154–20163.
- (34) Dechézelles, J.-F.; Aubert, T.; Grasset, F.; Cordier, S.; Barthou, C.; Schwob, C.; Maitre, A.; Vallée, R. A. L.; Cramail, H.; Ravaine, S. Fine tuning of emission through the engineering of colloidal crystals. *Phys. Chem. Chem. Phys.* **2010**, *12* (38), 11993–11999.
- (35) Kirakci, K.; Kubát, P.; Fejfarová, K.; Martinčík, J.; Nikl, M.; Lang, K. X-ray inducible luminescence and singlet oxygen sensitization by an octahedral molybdenum cluster compound: a new class of nanoscintillators. *Inorg. Chem.* **2016**, *55* (2), 803–809.
- (36) Amela-Cortes, M.; Paofai, S.; Cordier, S.; Folliot, H.; Molard, Y. Tuned Red NIR Phosphorescence of Polyurethane Hybrid Composites Embedding Metallic Nanoclusters for Oxygen Sensing. *Chem. Commun.* **2015**, *51* (38), 8177–8180.
- (37) Amela-Cortes, M.; Molard, Y.; Paofai, S.; Desert, A.; Duvail, J. L.; Naumov, N. G.; Cordier, S. Versatility of the Ionic Assembling Method to Design Highly Luminescent PMMA Nanocomposites Containing $[\text{M}_6\text{Q}_8\text{L}_6]^{n-}$ Octahedral Nano-building Blocks. *Dalton Trans.* **2016**, *45* (1), 237–245.

- (38) Thi Kim Nguyen, N.; Dubernet, M.; Matsui, Y.; Wilmet, M.; Shirahata, N.; Rydzek, G.; Dumait, N.; Amela-Cortes, M.; Renaud, A.; Cordier, S.; Molard, Y.; Grasset, F.; Uchikoshi, T. Transparent functional nanocomposite films based on octahedral metal clusters: synthesis by electrophoretic deposition process and characterization. *R. Soc. Open Sci.* **2019**, *6* (3), 181647.
- (39) Nguyen, N. T. K.; Renaud, A.; Dierre, B.; Bouteille, B.; Wilmet, M.; Dubernet, M.; Ohashi, N.; Grasset, F.; Uchikoshi, T. Extended Study on Electrophoretic Deposition Process of Inorganic Octahedral Metal Clusters: Advanced Multifunctional Transparent Nanocomposite Thin Films. *Bull. Chem. Soc. Jpn.* **2018**, *91* (12), 1763–1774.
- (40) Truong, T. G.; Dierre, B.; Grasset, F.; Saito, N.; Saito, N.; Nguyen, T. K. N.; Takahashi, K.; Uchikoshi, T.; Amela-Cortes, M.; Molard, Y.; Cordier, S.; Ohashi, N. Visible tunable lighting system based on polymer composites embedding ZnO and metallic clusters: from colloids to thin films. *Sci. Technol. Adv. Mater.* **2016**, *17* (1), 443–453.
- (41) Grant, J. T.; Carrero, C. A.; Goeltl, F.; Venegas, J.; Mueller, P.; Burt, S. P.; Specht, S. E.; McDermott, W. P.; Chieragato, A.; Hermans, I. Selective Oxidative Dehydrogenation of Propane to Propene using Boron Nitride Catalysts. *Science* **2016**, *354* (6319), 1570–1573.
- (42) Shi, L.; Wang, D.; Song, W.; Shao, D.; Zhang, W. P.; Lu, A. H. Edge-hydroxylated Boron Nitride for Oxidative Dehydrogenation of Propane to Propylene. *ChemCatChem* **2017**, *9* (10), 1788–1793.
- (43) Shi, L.; Wang, D.; Lu, A.-H. A Viewpoint on Catalytic Origin of Boron Nitride in Oxidative Dehydrogenation of Light Alkanes. *Chin. J. Catal.* **2018**, *39* (5), 908–913.
- (44) Tang, S.; Zhou, X.; Zhang, S.; Li, X.; Yang, T.; Hu, W.; Jiang, J.; Luo, Y. Metal-Free Boron Nitride Nanoribbon Catalysts for Electrochemical CO₂ Reduction: Combining High Activity and Selectivity. *ACS Appl. Mater. Interfaces* **2019**, *11* (1), 906–915.
- (45) Chen, H.; Yang, Z. Z.; Zhang, Z. H.; Chen, Z. T.; Chi, M. F.; Wang, S.; Fu, J.; Dai, S. Construction of a Nanoporous Highly Crystalline Hexagonal Boron Nitride from an Amorphous Precursor for Catalytic Dehydrogenation. *Angew. Chem., Int. Ed.* **2019**, *58* (31), 10626–10630.
- (46) Jiang, L. B.; Yuan, X. Z.; Zeng, G. M.; Wu, Z. B.; Liang, J.; Chen, X. H.; Leng, L. J.; Wang, H.; Wang, H. Metal-free Efficient Photocatalyst for Stable Visible-light Photocatalytic Degradation of Refractory Pollutant. *Appl. Catal., B* **2018**, *221*, 715–725.
- (47) Weng, Q. H.; Ide, Y.; Wang, X. B.; Wang, X.; Zhang, C.; Jiang, X. F.; Xue, Y. M.; Dai, P. C.; Komaguchi, K.; Bando, Y.; Golberg, D. Design of BN Porous Sheets with Richly Exposed (002) Plane Edges and Their Application as TiO₂ Visible Light Sensitizer. *Nano Energy* **2015**, *16*, 19–27.
- (48) Ide, Y.; Liu, F.; Zhang, J.; Kawamoto, N.; Komaguchi, K.; Bando, Y.; Golberg, D. Hybridization of Au Nanoparticle-loaded TiO₂ with BN Nanosheets for Efficient Solar-driven Photocatalysis. *J. Mater. Chem. A* **2014**, *2* (12), 4150–4156.
- (49) Ide, Y.; Nagao, K.; Saito, K.; Komaguchi, K.; Fuji, R.; Kogure, A.; Sugahara, Y.; Bando, Y.; Golberg, D. h-BN Nanosheets as Simple and Effective Additives to Largely Enhance the Activity of Au/TiO₂ Plasmonic Photocatalysts. *Phys. Chem. Chem. Phys.* **2016**, *18* (1), 79–83.
- (50) Kirakci, K.; Cordier, S.; Perrin, C. Synthesis and Characterization of Cs₂Mo₆X₁₄ (X = Br or I) Hexamolybdenum Cluster Halides: Efficient Mo-6 Cluster Precursors for Solution Chemistry Syntheses. *Z. Anorg. Allg. Chem.* **2005**, *631* (2–3), 411–416.
- (51) Nazarov, A. S.; Demin, V. N.; Grayfer, E. D.; Bulavchenko, A. I.; Arymbaeva, A. T.; Shin, H. J.; Choi, J. Y.; Fedorov, V. E. Functionalization and Dispersion of Hexagonal Boron Nitride (h-BN) Nanosheets Treated with Inorganic Reagents. *Chem. - Asian J.* **2012**, *7* (3), 554–560.
- (52) Sheldon, J. C. 208. Chloromolybdenum(II) Compounds. *J. Chem. Soc.* **1960**, 1007–1014.
- (53) Sheldon, J. C. 76. Bromo- and Iodo-molybdenum(II) Compounds. *J. Chem. Soc.* **1962**, 410–415.
- (54) Mikhaylov, M. A.; Abramov, P. A.; Komarov, V. Y.; Sokolov, M. N. Cluster Aqua/Hydroxocomplexes Supporting Extended Hydrogen Bonding Networks. Preparation and Structure of a Unique Series of Cluster Hydrates [Mo₆I₈(OH)₄(H₂O)₂]ⁿH₂O (n = 2, 12, 14). *Polyhedron* **2017**, *122*, 241–246.
- (55) Godet, C.; Ababou-Girard, S.; Fabre, B.; Molard, Y.; Fadjie-Djomkam, A. B.; Deputier, S.; Guilloux-Viry, M.; Cordier, S. Surface Immobilization of Mo₆I₈ Octahedral Cluster Cores on Functionalized Amorphous Carbon Using a Pyridine Complexation Strategy. *Diamond Relat. Mater.* **2015**, *55*, 131–138.
- (56) Ababou-Girard, S.; Cordier, S.; Fabre, B.; Molard, Y.; Perrin, C. Assembly of Hexamolybdenum Metallic Clusters on Silicon Surfaces. *ChemPhysChem* **2007**, *8* (14), 2086–2090.
- (57) Shi, Y. M.; Hamsen, C.; Jia, X. T.; Kim, K. K.; Reina, A.; Hofmann, M.; Hsu, A. L.; Zhang, K.; Li, H. N.; Juang, Z. Y.; Dresselhaus, M. S.; Li, L. J.; Kong, J. Synthesis of Few-Layer Hexagonal Boron Nitride Thin Film by Chemical Vapor Deposition. *Nano Lett.* **2010**, *10* (10), 4134–4139.
- (58) Yu, S. J.; Wang, X. X.; Pang, H. W.; Zhang, R.; Song, W. C.; Fu, D.; Hayat, T.; Wang, X. K. Boron Nitride-based Materials for the Removal of Pollutants from Aqueous Solutions: A Review. *Chem. Eng. J.* **2018**, *333*, 343–360.
- (59) Chen, F.; Zhao, J. C.; Hidaka, H. Highly Selective Deethylation of Rhodamine B: Adsorption and Photooxidation Pathways of the Dye on the TiO₂/SiO₂ Composite Photocatalyst. *Int. J. Photoenergy* **2003**, *5* (4), 209–217.
- (60) Hu, X. F.; Mohamood, T.; Ma, W. H.; Chen, C. C.; Zhao, J. C. Oxidative Decomposition of Rhodamine B Dye in the Presence of VO₂⁺ and/or Pt(IV) Under Visible Light Irradiation: N-deethylation, Chromophore Cleavage, and Mineralization. *J. Phys. Chem. B* **2006**, *110* (51), 26012–26018.
- (61) Mahlambi, M. M.; Mishra, A. K.; Mishra, S. B.; Krause, R. W.; Mamba, B. B.; Raichur, A. M. Comparison of Rhodamine B Degradation under UV Irradiation by Two Phases of Titania Nanophotocatalyst. *J. Therm. Anal. Calorim.* **2012**, *110* (2), 847–855.
- (62) Stengl, V.; Henych, J.; Slusna, M. h-BN-TiO₂ Nanocomposite for Photocatalytic Applications. *J. Nanomater.* **2016**, *2016*, 1.
- (63) Niki, E. Action of Ascorbic-Acid as a Scavenger of Active and Stable Oxygen Radicals. *Am. J. Clin. Nutr.* **1991**, *54* (6), 1119S–1124S.
- (64) Adams, G. E.; Boag, J. W.; Michael, B. D. Reactions of the Hydroxyl Radical. Part 2.—Determination of Absolute Rate Constants. *Trans. Faraday Soc.* **1965**, *61*, 1417–1424.
- (65) Katsumata, H.; Taniguchi, M.; Kaneco, S.; Suzuki, T. Photocatalytic Degradation of Bisphenol A by Ag₃PO₄ under Visible Light. *Catal. Commun.* **2013**, *34*, 30–34.
- (66) Si, H. B.; Lian, G.; Wang, J.; Li, L. Y.; Wang, Q. L.; Cui, D. L.; Wong, C. P. Synthesis of Few-Atomic-Layer BN Hollow Nanospheres and Their Applications as Nanocontainers and Catalyst Support Materials. *ACS Appl. Mater. Interfaces* **2016**, *8* (3), 1578–1582.